Spatio-temporal evolution of the H → L back transition

K. Miki,[1,2] P. H. Diamond,[1,3] L. Schmitz,[4] D. C. McDonald,[5] T. Estrada,[6] Ö. D. Gürcan,[7] and G. R. Tynan[3]
[1]*WCI Center for Fusion Theory, National Fusion Research Institute, Daejeon 305-333, South Korea*
[2]*Center for Computational Science and e-Systems, Japan Atomic Energy Agency, Chiba 277-8587, Japan*
[3]*Center for Momentum Transport and Flow Organization, University of California, San Diego, California 92093, USA*
[4]*University of California, Los Angeles, California 90095, USA*
[5]*JET-EFDA, Culham Centre for Fusion Energy, Arbingdon, United Kingdom*
[6]*Laboratorio Nacional de Fusión, Asociación Euratom-CIEMAT, Madrid, Spain*
[7]*LPP, Ecole Polytechnique, CNRS, France*

(Received 25 February 2013; accepted 4 June 2013; published online 28 June 2013)

Since ITER will operate close to threshold and with limited control, the H → L back transition is a topic important for machine operations as well as physics. Using a reduced mesoscale model [Miki *et al.*, Phys. Plasmas **19**, 092306 (2012)], we investigate ELM-free H → L back transition dynamics in order to isolate transport physics effects. Model studies indicate that turbulence spreading is the key process which triggers the back transition. The transition involves a feedback loop linking turbulence and profiles. The I-phase appears during the back transition following a slow power ramp down, while fast ramp-downs reveal a single burst of zonal flow during the back transition. The I-phase nucleates at the pedestal shoulder, as this is the site of the residual turbulence in H-mode. Hysteresis in the profile gradient scale length is characterized by the Nusselt number, where $\mathrm{Nu} = \chi_{i,turb}/\chi_{i,neo}$. Relative hysteresis of temperature gradient vs density gradient is sensitive to the pedestal Prandtl number, where $\mathrm{Pr}_{ped} = D_{ped}/\chi_{i,neo}$. We expect the H-mode to be somewhat more resilient in density than in temperature. © *2013 AIP Publishing LLC*. [http://dx.doi.org/10.1063/1.4812555]

I. INTRODUCTION

Understanding the L → H and H → L transitions is crucial to successful ITER operation. There is growing interest in H → L back transitions, since ITER will operate close to threshold ($P \sim P_T$), and with limited control ($\tau_{resp} > \tau_E$, where τ_{resp} is the response time of the control system and τ_E is the energy confinement time).[1] Thus, understanding H → L transition dynamics and hysteresis is critical. The nature of hysteresis also gives a fundamental clue as to the "order" of the L → H phase transition, i.e., first vs. second. Some of the major questions concerning H → L back transition dynamics are

i) Does the plasma re-visit I-phase in the course of the back transition? Doing so might ensure a "soft landing" after the back transition—an outcome which clearly is desirable.
ii) What is the fundamental dynamical process of the back transition? Is there a feedback loop?
iii) How do we describe and quantify hysteresis? How do profiles affect hysteresis? Which transport channel exhibits the strongest hysteresis?

Here, we use a reduced mesoscale model[2] to investigate these questions. We focus on ELM-free transition dynamics—i.e., we follow a scenario of a ramp down from $P > P_{crit}$. This approach allows us to separate transport dynamics from MHD and edge localized mode (ELM) physics. Similar physical experiments (i.e., studies of ELM free back-transitions) would be enlightening, and should be pursued.

Regarding the first question concerning the dynamics of the H → L back transition, recent results from DBS studies on DIII-D suggest that back transition limit-cycle oscillations (LCOs) do exist[3]—the plasma can revisit the I-phase during the back transition. See the results from DIII-D, shown in Fig. 1. The system clearly passes through the I-phase during the H → L back transition. Indeed, the LCO behavior seen in the forward transition occurring after 3500 ms is mirrored in the back transition (3030-3500 ms); i.e., as the L → H forward transition progresses, the $E \times B$ shear flow oscillation frequency decreases, while the LCO oscillation frequency *increases* as the H → L back transition progresses. This is because strong $E \times B$ shear suppresses turbulence growth and so tends to slow down the rise of turbulence during the LCO. Thus, the LCO frequency decreases during the forward transition but increases during the back transition. The total $E \times B$ velocity peaks at the beginning of the back I-phase, but then decreases, as seen in Fig. 1(d).

Generally, hysteresis is a dependence of a system not only on its current state but also on its past history.[8] To predict its future development, we must know either the system's initial state or its history. If hysteresis exists for a system, depending on its history, the system can manifest either of two distinct solutions (e.g., L-mode and H-mode), for exactly the same parameters. Therefore, the coexistence of the two possible states is essential.

The question of hysteresis is both highly relevant to ITER and fundamental to the nature of the bifurcation transition, and thus is of great interest. However, it is curious to note that in distinct contrast to the plethora of papers on L → H dynamics and the extensive databases for threshold power, there are very few, if any, dedicated studies of back transition dynamics and no databases for hysteresis.

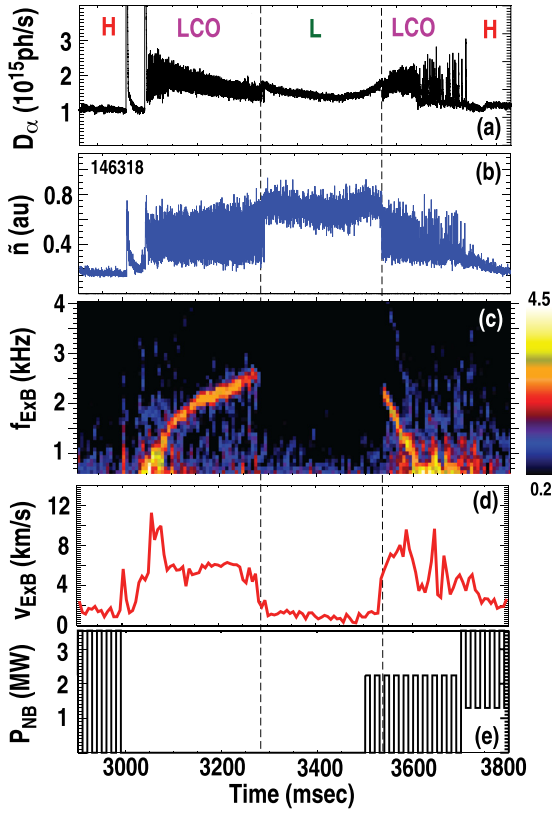

FIG. 1. In DIII-D, temporal evolution of (a) D_α lower divertor signal; (b) density fluctuation level; (c) frequency spectrum of $E \times B$ velocity fluctuations (including zonal flow and diamagnetic flow fluctuations), (d) magnitude of oscillating $E \times B$ velocity (all measured 0.5 cm inside the LCFS); (e) neutral beam power during a sequence of H → I(LCO), I → L, L → I, and I → H transitions.

Indeed, a fundamental question concerning hysteresis is how to quantify it in terms of local *physical* quantities, other than the global engineering parameter definition $P_{L\to H}/P_{H\to L}$ (e.g., Refs. 4 and 5)!? Of course, we realize that the physical underpinning of hysteresis phenomena is the difference in transport between the L (strongly turbulent) and H (neoclassical/weakly turbulent) regimes.[6] Experimental measurement of local edge electron parameters during power ramp-up and down indicates different transition paths between L → H and H → L transitions.[4,7] However, more detailed questions concerning hysteresis, such as which channel? what quantity? etc., remain unanswered.

To this end, we thus construct a hysteresis loop for the *local* edge profile gradient. These change drastically during an L → H transition. We show then that Nusselt number $\mathrm{Nu}_A = D_{A,L}/D_{A,ped}$ correlates well with the area of that hysteresis loop. Note that $D_{A,ped}$ is the *effective* pedestal diffusivity. In the case of $T_i, D_{T_i,ped} \cong \chi_{i,neo}$ but for density $D_{n,ped} = D_{n,resid}$, the residual turbulent transport in H-mode.

We expect hysteresis to be *relative*, i.e., some gradients will evolve differently from other ones in the L → H and H → L transitions. The meaning of relative hysteresis follows from that of hysteresis. We have defined hysteresis as the phenomenon of coexistence of two states for a single value of the control parameter. Thus, for "relative" hysteresis of two quantities A, B (here, $A = \nabla n$ and $B = \nabla T$ is one possibility), we mean the coexistence of two possible values of B for a single value of A. Note that relative hysteresis is related fundamentally to *stationary states*, and not relaxation. However, the existence of relative hysteresis can indeed give the appearance of a difference in evolution between A and B.

Relative hysteresis is naturally described by pedestal or residual Prandtl number $\mathrm{Pr}_{ped} \equiv D_{n,ped}/\chi_{i,ped}$, etc. Relative hysteresis should appear as a loop of finite area in the phase portrait of $1/L_n$ vs $1/L_{T_i}$, with area scaling inversely with $\mathrm{Pr}_{resid} = D_{ped}/\chi_{i,neo}$. Here, L_A is a characteristic length, defined as $L_A = |(1/A(r))(\mathrm{d}A(r)/\mathrm{d}r)|^{-1}$. Similar aspects of relative hysteresis, with respect to toroidal momentum $1/L_{V_\phi}$ vs $1/L_{T_i}$, have been discussed in the context of internal transport barrier (ITB) transitions. One case is related to the LHD experiments,[9] and the other is from numerical gyro-fluid simulations.[10] Thus, the fundamental investigation of relative hysteresis and its residual Prandtl number scaling is another important issue. Measurement of relative hysteresis is an additional tool to discriminate between the L → H and H → L transitions and gives additional information about the underlying pedestal physics. The study of relative hysteresis is useful in understanding how the H → L back transition evolves and which transport channel (and associated profile) is most important to it.

In this paper, we present the first theoretically based model studies of back-transition dynamics. We focus on three key questions, which are: (i) does the plasma re-visit I-phase during the back transition and what is the duration of the oscillations? (ii) what is the trigger mechanism and feedback loop physics of the back transition, (iii) how do we best quantify hysteresis? We utilize a simple model which separates transport from ELM physics.

The remainder of this paper is organized as follows. In Sec. II, we review the reduced mesoscale model, and show examples of the L → H transition. In Sec. III, we present numerical results of the L → H → L transitions, and details of the feedback loop discovered in the back transition dynamics. In Sec. IV, we discuss and characterize hysteresis and relative hysteresis. In Sec. V, we discuss model predictions for the hysteresis. In Sec. VI, we conclude and discuss remaining issues.

II. MODEL DESCRIPTION

We have developed a 5-field reduced mesoscale (envelope) model which evolves turbulence intensity (I), mean square zonal flow shear ($E_0 = V'^2_{ZF}$), ion pressure (p) and density (n) profiles, and mean poloidal mass flow ($\langle V_\theta \rangle$) in radius r and time, all in cylindrical geometry. The details of the model are discussed in Ref. 2. The model equations are

$$\partial_t I = I(\gamma_L - \Delta\omega I - \alpha_0 E_0 - \alpha_V E_V) + \chi_N \partial_r (I \partial_r I), \quad (1)$$

$$\partial_t E_0 = [\alpha_0 I/(1 + \zeta_0 E_V) - \gamma_{\mathrm{damp}}] E_0, \quad (2)$$

$$\partial_t p + (1/r)\partial_r [-r(\chi_{\mathrm{i,neo}} + \chi_{\mathrm{i,turb}})\partial_r p] = Q_a \exp(-r^2/2L^2_{\mathrm{h,dep}}), \quad (3)$$

$$\partial_t n + (1/r)\partial_r[-r[(D_{\text{ped}} + D_{\text{turb}})\partial_r n + V_n n]] = \Gamma_a \frac{a - r + d_a}{L_{\text{dep}}^2} \exp\left[-\frac{(a - r + d_a)^2}{2L_{\text{dep}}^2}\right], \quad (4)$$

$$\frac{\partial \langle v_\theta \rangle}{\partial t} = -\alpha_5 \frac{\gamma_L}{\omega_*} c_s^2 \frac{\partial I}{\partial x} - \mu_0^{(\text{neo})} \nu_{ii} q^2 R^2 \left(\langle v_\theta \rangle + 1.17 c_s \frac{\rho_i}{L_T} \right), \quad (5)$$

$$\langle V_E \rangle' = \frac{1}{eB}\left[-\frac{n'p'}{n^2} + \frac{p''}{n}\right] - a\langle v_\theta \rangle'. \quad (6)$$

The notation and details of the parameters are described in Ref. 2. Here, we briefly outline the essential framework. Equations (1) and (2) represent a one prey (turbulence intensity)—two predator (zonal flow and mean flow) model, motivated by Ref. 11. We include nonlinear turbulence spreading. The mean flow shear $E_V = \langle V_E \rangle'^2$ modulates Reynolds drive in the zonal flow evolution. This inhibition is characterized by the factor ζ_0. Equations (3) and (4) represent heat and particle transport evolution. The diffusion terms consists of the turbulent $\chi_{\text{i,turb}}, D_{\text{turb}}$, and neoclassical (pedestal) transport $\chi_{\text{i,neo}}$, D_{ped}. Here, the turbulent transport is proportional to the turbulence intensity, $\chi_{\text{i,turb}} = D_{\text{turb}} \propto I$, while the neoclassical transport is independent of turbulence. We include the particle pinch in the density evolution. The pinch velocity consists of turbulent equipartition pinch (TEP) and thermoelectric contributions. The particle pinch causes density profile peaking. We do not include a heat pinch in the pressure evolution, because the heat source is applied in the core, and we are not concerned with global temperature profile structure. In Eq. (5), we describe the evolution of poloidal mass flow. The poloidal mass flow is driven by turbulent stress and neoclassical dynamics. The radial force balance Eq. (6) is used to couple the mean $E \times B$ flow and profile (pressure and density) gradients. The radial force balance equation includes the pressure curvature, i.e., the second derivative of the pressure profile, and poloidal momentum evolution. Note that we here neglect toroidal momentum evolution, for simplicity. We impose free edge boundary condition on I, E_0, and $\langle v_\theta \rangle$, by neglecting scrape-off-layer- (SOL-) edge coupling. p and n are set to be fixed on the edge boundary. We also neglect any MHD activity, such as ELMs.

We examine the L → H transition with different heating histories. In Ref. 2, the L → H or L → I → H transition was achieved with a monotonically increasing (fast or slow) heat flux. However, experiments cannot always reproduce such monotonic ramps. We here confirm that the difference in heating history does not change the physics of the L → I → H/L → H transition. Thus, we apply a piecewise continuous heating power, with a step-like change in time. Fig. 2(a) shows the L → H transition evolving through the I-phase. In the intermediate time regime, during $(1.0 < t < 2.0)[10^5 a/c_s]$, we encounter a LCO by selecting an intermediate value of the heat flux between the L and H values. For such heating, the fixed point for which turbulence and zonal flow coexist is destabilized by the mean flow competition, so that the LCO is established as a stationary (long-lived), state. This observation indicates that the I-phase is a distinct, physical regime, fundamentally different than the L- or H-mode.

Further increasing the heat flux above a threshold, the L → H transition occurs. At the L → H transition, the turbulence and zonal flow suddenly collapse, and the increasing mean flow is locked in for $r/a > 0.9$. Inside the pedestal shoulder, for $r/a < 0.9$, residual turbulence and zonal flow persist, even after the transition. This behavior is identical to that for the case where the heat flux increases slowly, as described in Ref. 2.

Fig. 2(b) shows an L → H transition without the I-phase. In the intermediate time regime $(1.0 < t < 2.0)[10^4\, a/c_s]$, the weak heat flux cannot excite mean flow shear sufficient to trigger the I-phase. At $t = 2.0 \times 10^4 (a/c_s)$, we change Q_a above the power threshold, starting from the L-mode state. Then, a single burst of zonal flow shearing occurs and triggers the L → H transition at $t = 2.1 \times 10^4 (a/c_s)$. This behavior is similar to the case with rapidly increasing heat flux.

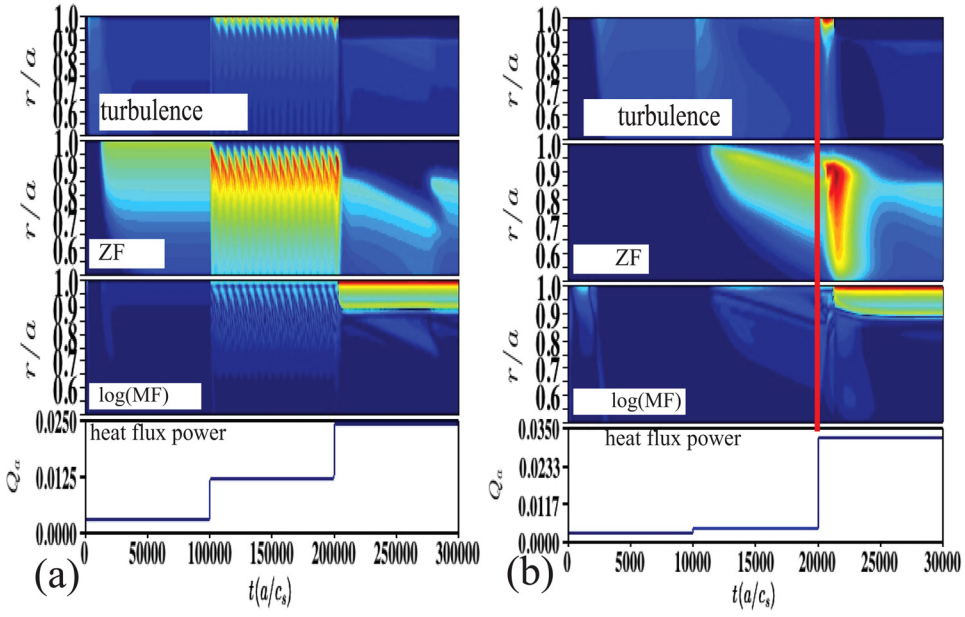

FIG. 2. Spatio-temporal evolution of turbulence intensity, zonal flow energy, mean flow $\langle v_E \rangle'^2$, and heat flux input Q_a, for different heating evolutions. (a) The case for the step-like heat flux increase from the marginal power (i.e., I-phase, as shown), above the L → H power threshold, (revealing L → H transition). (b) The case for the step-like heat flux rising above the L → H power threshold from the L-mode at $t = 2.0 \times 10^4 (a/c_s)$. The L → H transition occurs after a single burst of zonal flow at $t = 2.1 \times 10^4 (a/c_s)$.

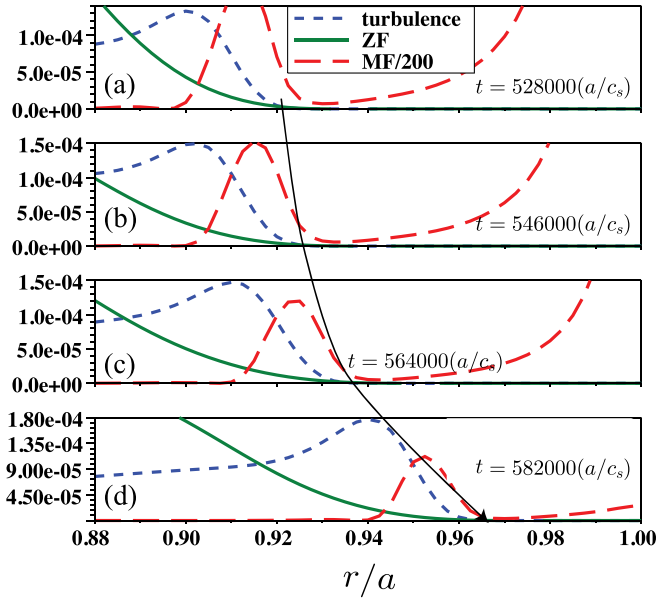

FIG. 3. Profiles of turbulence intensity, zonal flow energy, and mean flow shearing energy as a function of radius r/a, for a time interval $\Delta t = 18\,000(a/c_s)$ from (a) through (d). As indicated by the arrow, the turbulence spreading advances from the core to the edge region, through the H → L back transition.

We conclude that the appearance and duration of the pre-transition LCO should be sensitive to the heating below the L → H power threshold, as is discussed in the previous work of Refs. 2, 12, and 13.

III. EVOLUTION OF THE H → L BACK TRANSITION

In this section, we study model results from cases with heat flux first increasing above the L → H threshold and then decreasing. For a decreasing heat flux, the system will return to the L-mode. We first focus on the dynamics of the back transition.

Fig. 3 shows that the back transition is fundamentally a process of turbulence spreading into a quiescent region. The turbulent region is the core and the quiescent region is the pedestal. Fig. 3 shows that the turbulent core advances into the pedestal (c.f. follow the evolution of the dashed blue curve). It also shows the drop in the mean shear (red curve), as the region of maximal flow curvature—the "corner," where the turbulent core connects to the steep gradient pedestal—collapses toward the last closed flux surface (LCFS). Finally, we see that the zonal flow (green curve) is dragged along by the turbulence, as it must be, since the zonal flow is driven by turbulence. Thus, we see that the back transition is indeed a process whereby the interface between the turbulent core and the quiescent or neoclassical pedestal advances toward the boundary. This turbulence spreading process is regulated by nonlinear couplings (i.e., $\chi_N I$ in the intensity equation (Eq. (1)), zonal and mean flow control parameters (i.e., damping), and the transport coefficients which determine the mean flow shear. Such turbulence spreading has been observed in back-transition experiments in TJ-II.[14] There, the advance of a turbulence front into the E_r shear layer was observed. They also observed the drop of the E_r shear during the process.

As to the question of the feedback loop mechanism, *turbulence spreading* is the key process. When the heat flux Q drops, profile gradients ∇p and ∇T decrease according to Eq. (3). As ∇T decreases, ∇n decreases due to the decrease of the thermoelectric particle pinch velocity, which is proportional to L_T^{-1}. As ∇p, ∇T, and ∇n decrease, the mean flow shear $\langle v_E \rangle'^2$ decreases according to Eq. (6). Then, turbulence advances into the quiescent region. When the local turbulence intensity increases, the local transport also increases. The increased transport then decreases the profile gradients, such as ∇p and ∇n. This, in turn, leads to a decrease of mean flow shear, which then allows further turbulence invasion. This is how the positive feedback loop develops, illustrated in Fig. 4.

Fig. 5 shows several cases of the spatio-temporal evolution of turbulence, zonal flow, and mean flow through the L → H → L transitions. First, heat flux *monotonically* increases above the threshold, so the L → H transition occurs. Next, the heat flux monotonically decreases to the original level, and the system returns to the L-mode. Here, we investigate the several cases with different heating histories.

Figure 5(b) shows a slower ramp down than the case Fig. 5(a), while Figs. 5(c) and 5(d) show cases with faster ramp downs. Fig. 5(b) shows clearly that an I-phase and/or LCO appear during the evolution from the H- to L-mode. In the forward L → H transition, as shown in Fig. 2(a), the pre-transition LCO is nucleated near the LCFS, as this is where the turbulence intensity gradient (and so the Reynolds force) is largest. However, during the back transition, *the LCO is nucleated at the pedestal shoulder*, since that is the location of the residual turbulence in the H-mode. This is related to the fundamental character of the back transition, which is a process of turbulence penetration from an active core into the quiescent pedestal. During the forward L → H transition, the LCO frequency decreases. Not surprisingly, the LCO frequency *increases* during the back I-phase, since $\langle V_E \rangle'$ drops so turbulence can increase faster. This is a similar trend to recent experimental results from DIII-D (see Fig. 1). The region of zonal flow and turbulence activity slowly expands toward the LCFS. The LCO induces ∇p oscillations which in turn drive D_α bursts. These, then, may correspond to the

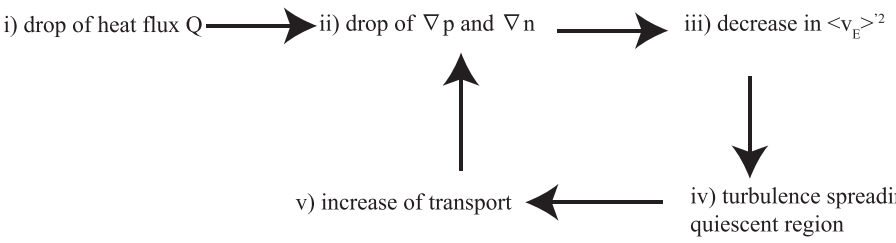

FIG. 4. Illustration of the feedback loop during the H → L back transition. Process proceeds from (i) through (v) and then returns to (ii) and thus closes the loop.

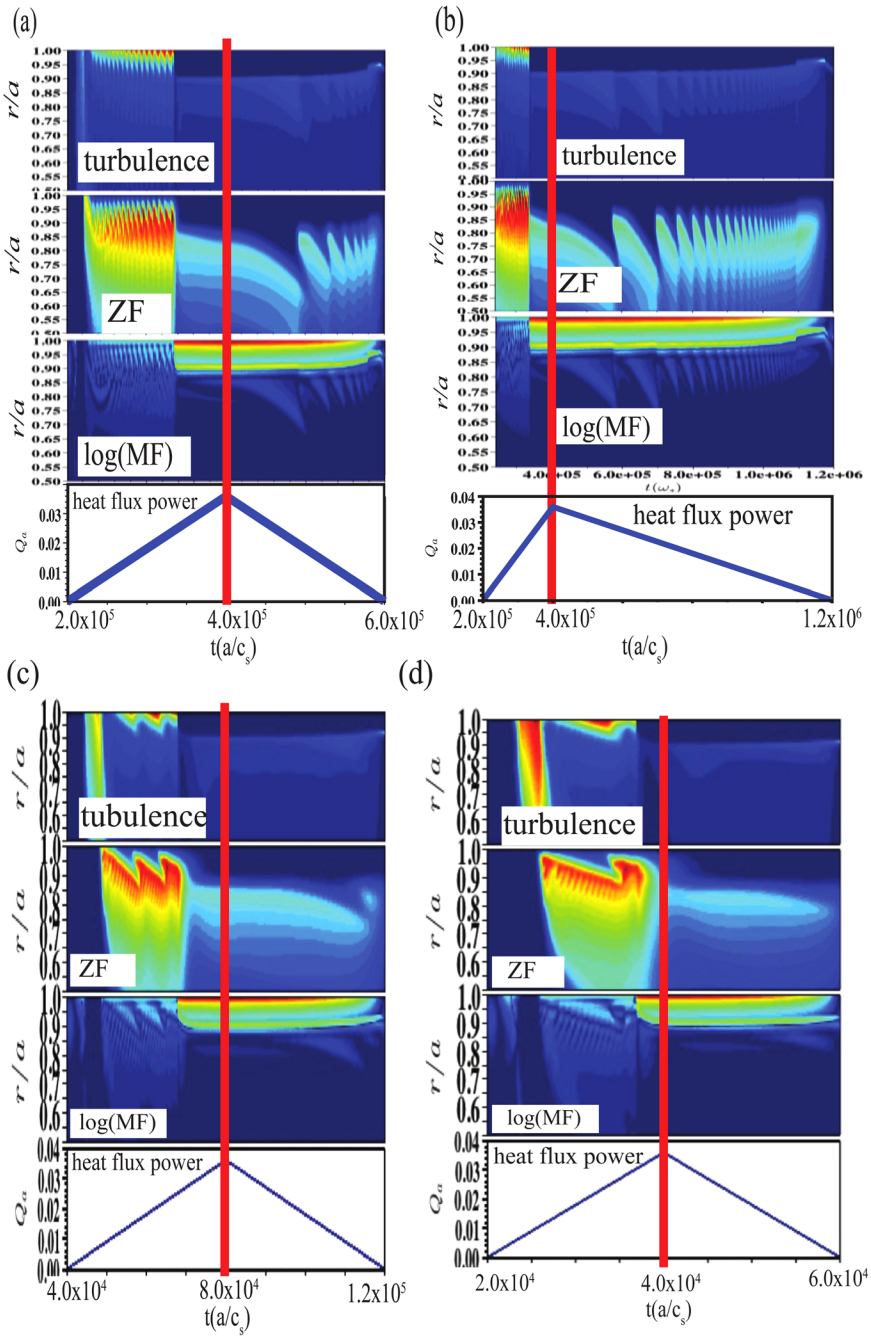

FIG. 5. Spatio-temporal evolution of turbulence, zonal flow energy, mean flow, and heat flux, in cases with (a) a ramp at a reference speed, (b) 4 times slower ramp-down rate, (c) 5 times faster ramp-up rate, and (d) 10 times faster ramp-up. The LCO appears for cases with a slower ramp rate (i.e., (a) and (b)), while the LCO is compressed into a single burst of zonal flow for cases with faster ramp ((c) and (d)).

so called "Type-III ELMs"[15] reported during the decay of β_p at the back transition.

Figure 5(b) examines the same case for a ramp-down which is four times slower than the case of Fig. 5(a). Results are similar, but the I-phase is extended. Figs. 5(c) and 5(d) show ramp downs which are 5 and 10 times faster, respectively. There, at most a few bursts of zonal flow activity occur, and the LCO is compressed by the fast ramp. The collapse to the L-mode proceeds quickly. Thus, we predict that the "landing" after the back-transition will not always be "soft," since the duration of the back-transition I-phase depends upon the rate of power ramp-down.

IV. MODEL STUDIES OF HYSTERESIS

The model essentially exhibits two distinct states, i.e., L-mode and H-mode.[11,16] Based on the Kim-Diamond model (Eqs. (1) and (2)), L-mode is defined as the state with finite levels of the turbulence and zonal flow. Since $D_{\text{turb}}, \chi_{\text{i,turb}} \gg D_{\text{neo}}, \chi_{\text{i,neo}}$ is satisfied there, turbulent transport determines the (gentle) profile gradients. In H-mode, the levels of turbulence and zonal flow are essentially zero. Since the surviving $D_{\text{neo}}, \chi_{\text{i,neo}}$ are *small*, the pedestal (neoclassical) transport allows steep profile gradients. Both L and H branches of the Q vs. ∇T curve are stable, indicating bistability. There hysteresis appears, and depends on the history of heating.[6]

In this section, we study the hysteresis in scale lengths L_n, L_T, L_p. We also examine hysteresis in the profile quantities p, n, T, for comparison. The studies are straightforward (i.e., using simple ramps up, then down) and the net strength of hysteresis is calculated by measurement of the area of the hysteresis loop at a specific location in the pedestal, (typically $r/a = 0.95$). We systematically calculate the area of the

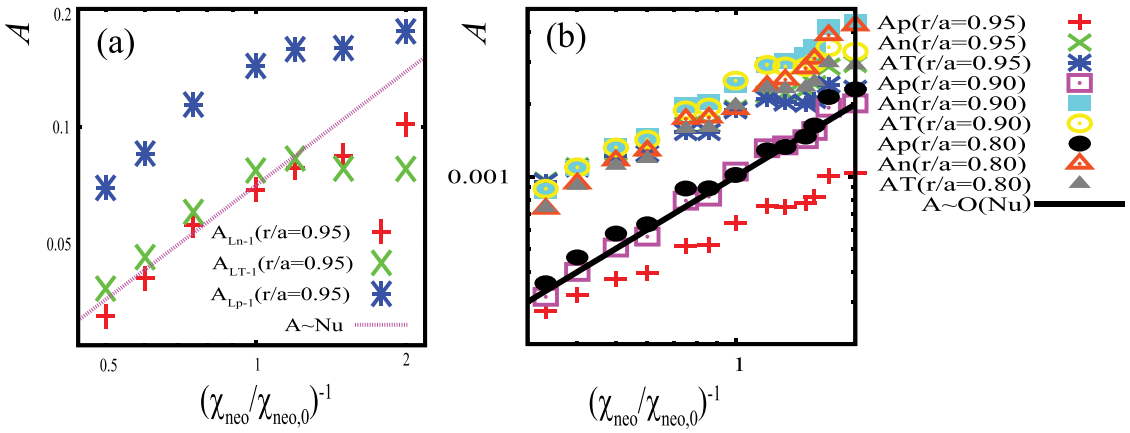

FIG. 6. The figure shows, as a function of $(\chi_{neo}/\chi_{neo,0})^{-1}$, the area of hysteresis loops in (a) scale lengths (L_n^{-1}, L_T^{-1}, L_p^{-1}), and (b) quantities (p, n, T) for various radial locations ($r/a = 0.95$: in the pedestal, $r/a = 0.9$: on the top of pedestal, and $r/a = 0.8$: inside of the pedestal shoulder). Both hystereses track the scaling $A \sim \mathrm{Nu}$, as shown by the red or black bold lines.

hysteresis loop, using the following path integration through the heating power (Q_a) ramp:

$$A_f = -\oint f \, \mathrm{d}Q_a, \quad (f = L_p^{-1}, L_n^{-1}, L_T^{-1}, p, n, T). \tag{7}$$

Figure 6(a) shows that the measured strength of hysteresis indeed scales in proportion to Nusselt number, which varies as $(\chi_{i,neo}/\chi_{i,neo,0})^{-1}$. The hystereses are obtained from loop areas for the inverse scale lengths plotted against the heat flux. Here, $\chi_{i,ped} \sim D_{n,ped} \sim \chi_{i,neo}$, through $D_{n,ped}$ and $\chi_{i,neo}$ differ by a numerical factor. $\chi_{i,neo,0}$ is a normalization factor. The evident deviation from linear proportionality of hysteresis to Nu at large Nu is likely due to difficulties in accurate measurement of loop area in that extreme limit. We note that the Nu proportionality of the area of the (hysteresis) loop in the inverse scale lengths is relevant only within the pedestal ($r/a \gtrsim 0.9$).[17] The hysteresis outside of the pedestal has no relevance to Nu proportionality, since there is no local transition. Fig. 6(b) plots the area of hysteresis in *the profile quantities*, as a function of $(\chi_{i,neo}/\chi_{i,neo,0})^{-1}$. The measured hysteresis also tracks the Nusselt number, as $(\chi_{i,neo}/\chi_{i,neo,0})^{-1}$ varies, for all radial locations (at least) within the barrier.

Figure 7 shows the *relative* hysteresis of $1/L_n$ and $1/L_T$, for different values of the pedestal Prandtl number, $\mathrm{Pr}_{ped} \equiv D_{n,ped}/\chi_{i,neo}$. The blue plots in the lower region represent the I-phase. In the I-phase, L_T^{-1} oscillates around L_n^{-1}, as the model sets $\chi_{i,turb} = D_{turb}$. On the other hand, in the H-mode, (plotted in red), $L_n^{-1} > L_T^{-1}$. Since the pedestal transport is different for particles and heat, (i.e., $D_{ped} < \chi_{i,neo}$), the pedestal particle barrier relaxes more slowly than the heat transport barrier does. Since the ramp-down speed is chosen to be slow enough to eliminate the effect of rate-dependent hysteresis, relative hysteresis is *not* a kind of rate-dependent hysteresis.[8] Relative hysteresis is characterized by the two distinct states, i.e., $L_T^{-1} \sim L_n^{-1}$ in L-mode and $L_T^{-1} < L_n^{-1}$ in H-mode. Thus, this behavior originates from the difference between states of the L- and H-modes in different profiles (density or temperature). As compared to Figs. 7(a)–7(c), relative hysteresis is evident and increases with $1/\mathrm{Pr}_{ped}$, as expected. Finite relative hysteresis implies that the H → L relaxation dynamics will not be the same for all quantities.

Figs. 8(a)–8(c) show hysteresis loops in plots of *scale lengths* $1/L_p$, $1/L_n$, and $1/L_{T_i}$ vs heat flux Q, while Figs. 8(d)–8(f) show the corresponding loops for *quantities* p, n, T. The I-phase behavior appears as an oscillation in the lower region. The L → H transition appears as a jump of the trace from the lower to the upper curve of $1/L$. As the heat flux decreases from the top, above the power threshold, the plots will follow the upper path. In the I-phase, the turbulent transport is dominant ($\chi_{i,turb} \gg \chi_{neo}$). On the other hand, in the H-mode pedestal, the neoclassical transport is dominant ($\chi_{neo} \gg \chi_{i,turb}$). Thus, the inverse scale lengths in the I-phase should be lower than those in the H-mode pedestal. The quantities in the I-phase are lower than those in the H-mode. Additionally, some slight oscillation in the loops, due to an

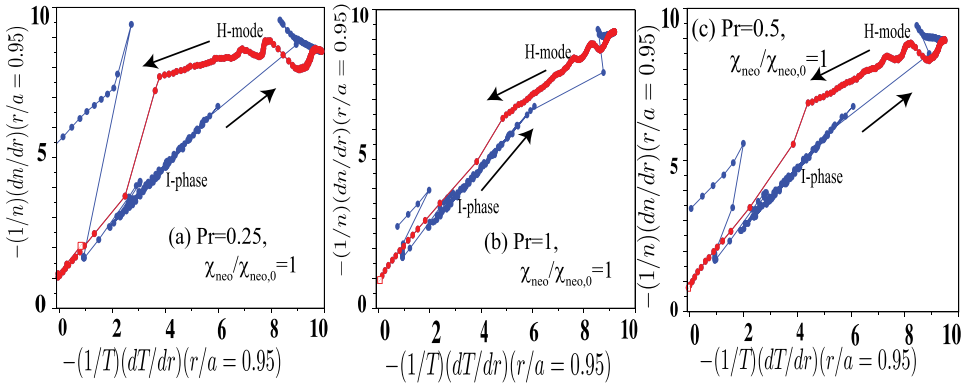

FIG. 7. Relative hysteresis in L_T^{-1} vs L_n^{-1} at $r/a = 0.95$, with different Prandtl numbers. Blue plots in $L_T^{-1} \sim L_n^{-1}$ indicate the evolution through the L → H transition, while red plots in $L_T^{-1} \lesssim L_n^{-1}$ indicate the evolution through the H → L back transition.

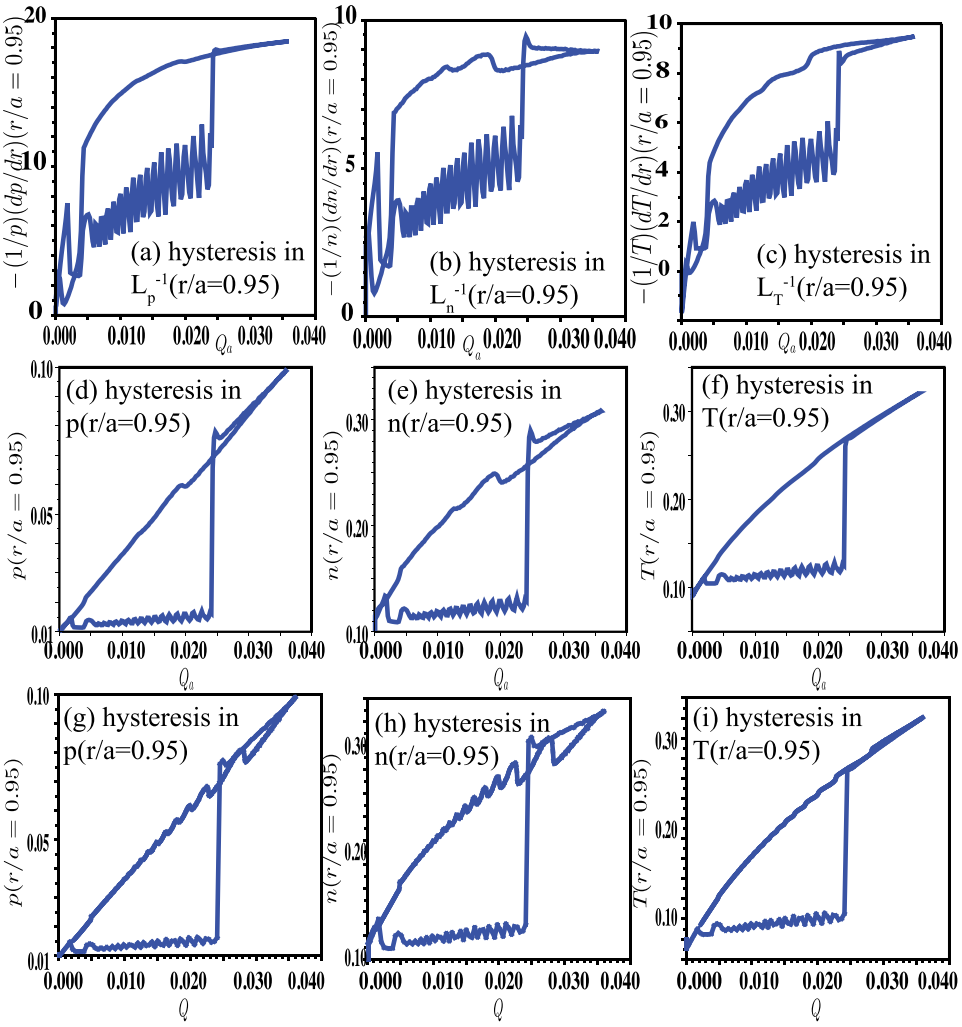

FIG. 8. Various hysteresis loops plotted as inverse scale lengths: (a) L_p^{-1}, (b) L_n^{-1}, (c) L_T^{-1} and profile quantities: ((d) and (g)) p, ((e) and (h)) n, and ((f) and (i)) T, at $r/a = 0.95$ (in the pedestal), vs heat flux intensity Q_a. Hystereses in gradient, (a)-(c), exhibit rectangular loops. On the other hand, those in profile quantities, (d)-(f), exhibit triangular loops. (g)-(i) Corresponds to the case with 4 times slower ramp-down (i.e., Fig. 5(b)).

LCO on the pedestal shoulder, is observed. These oscillations in back transition are sensitive to the ramp-down speed. As shown in Figs. 8(g)–8(i), the case with a 4 times slower ramp-down speed (see also Fig. 5(b)) shows a clearer LCO during the back transition. For hystereses in scale lengths (Figs. 8(a)–8(c)), the drop of the traces onto the lower path occurs when the turbulence front arrives at the radial location ($r/a = 0.95$) of observation. The lower trace corresponds to that of L-mode evolution. In case of hystereses in the quantities, symptoms of an abrupt local H → L back transition are not observed.

Interestingly, the gradient scale length hysteresis plots clearly *differ* from the quantity hysteresis plots. The former has an approximately rectangular shape, while the latter are roughly triangular. For the first case, the inverse scale length drops locally when the H → L back transition occurs, while for the latter, the quantity just smoothly decreases from H-mode to L-mode. Thus, quantity gradients (i.e., ∇p) give more insight into the back transition evolution than do the quantities (i.e., p) themselves. Of course, there is no *a-priori* reason to expect these two sets of loops to be equivalent. This observation illustrates the need to identify the most physically relevant quantities to define hysteresis in terms of. Not all definitions are equivalent! Local quantities surely give more insight into dynamics of the back transition than do macroscopic parameters.

We explore the macro-micro connection in Fig. 9. The dependence of zonal flow damping on ion collisionality is related to dependence on $\chi_{\mathrm{i,neo}}$. Thus, for equal ramp down rates, there should be a relation between $\chi_{\mathrm{i,neo}}$ and the back-I phase LCO frequency. This is confirmed in Fig. 9, which shows a higher LCO frequency for larger $\chi_{\mathrm{i,neo}}$ (indicative of smaller Nu).

V. DISCUSSION OF HYSTERESIS

Based on the model (Eqs. (1)–(6)), we present a simple theoretical framework for hysteresis. The stationary state of the density and pressure gradients incorporates the particle pinch, as well as turbulent and/or neoclassical diffusion effects. Using Eqs. (3) and (4), we calculate the stationary ($\partial/\partial t = 0$) profiles at a chosen edge location $r = x$. Integrating r over $[0, x]$ in Eqs. (3) and (4), we obtain

$$\left[-D\frac{\partial n(x)}{\partial r} + V_n n(x)\right] = S, \tag{8}$$

$$-\chi\frac{\partial p(x)}{\partial r} = Q, \tag{9}$$

where $Q = (1/x)\int_0^x rQ_a \exp(-r^2/2L_{\mathrm{dep,h}}^2)\mathrm{d}r$, and $S = (1/x)\int_0^x r\Gamma_a(a-r+d_a)/L_{\mathrm{dep}}^2 \exp[-(a-r+d_a)^2/(2L_{\mathrm{dep}}^2)]\mathrm{d}r$. Here, $D = D_{\mathrm{ped}} + D_{\mathrm{turb}}$, and $\chi = \chi_{\mathrm{neo}} + \chi_{\mathrm{i,turb}}$. The particle pinch

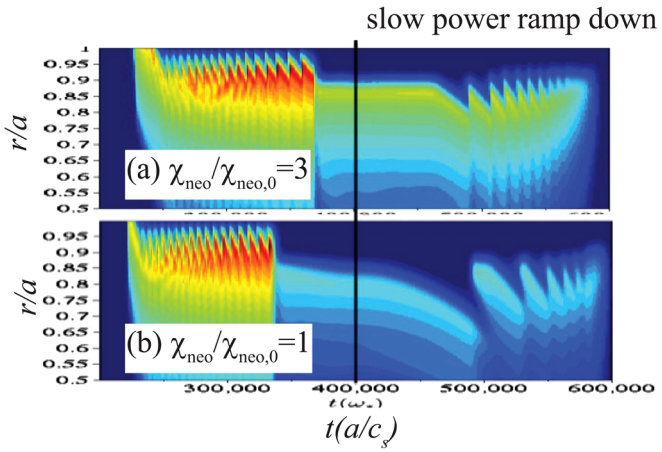

FIG. 9. Spatio-temporal evolution of zonal flow energy in the back transition with different χ_{neo}: (a) $\chi_{neo}/\chi_{neo,0} = 3$ and (b) $\chi_{neo}/\chi_{neo,0} = 1$. Back-transition I-phase behaves differently in χ_{neo}. Lower χ_{neo} exhibits relatively lower limit-cycle oscillation frequency in the back transition.

velocity is simply $V_n = -DL_{T_i}^{-1}$, where we neglect the TEP pinch, since $L_{T_i} \ll R$ in the pedestal. We assume $ST_i/Q \equiv \varepsilon \ll 1$. We rewrite Eqs.(8) and (9), in terms of gradient scale lengths,

$$L_n^{-1} = L_{T_i}^{-1} + \frac{S/n}{D_{\rm ped} + D_{\rm turb}}, \tag{10}$$

$$L_p^{-1} = \frac{Q/p}{\chi_{\rm neo} + \chi_{\rm i,turb}}. \tag{11}$$

Noting the identity, $L_{T_i}^{-1} = L_p^{-1} - L_n^{-1}$, we then obtain the results

$$L_{T_i}^{-1} = \frac{1}{2}\left[\frac{Q/p}{\chi_{\rm neo} + \chi_{\rm i,turb}} - \frac{S/n}{D_{\rm ped} + D_{\rm turb}}\right], \tag{12}$$

$$L_n^{-1} = \frac{1}{2}\left[\frac{Q/p}{\chi_{\rm neo} + \chi_{\rm i,turb}} + \frac{S/n}{D_{\rm ped} + D_{\rm turb}}\right]. \tag{13}$$

As is mentioned in Sec. IV, the ratio $L_{\rm ped}^{-1}/L_{\rm turb}^{-1}$ (scale length in pedestal/scale length in L-mode state) is a reasonable parameter with which to measure the strength of hysteresis. Using Eq. (11), we identify the proportionality of $P_p \equiv L_{p,\rm ped}^{-1}/L_{p,\rm turb}^{-1}$ to the Nusselt number, to obtain

$$P_p = \frac{(Q/p_{\rm neo})/\chi_{\rm neo}}{(Q/p_{\rm turb})/\chi_{\rm i,turb}} = \frac{\chi_{\rm i,turb}p_{\rm turb}}{\chi_{\rm neo}p_{\rm neo}} \sim {\rm Nu}. \tag{14}$$

Here, we assume $\chi_{\rm i,neo}, D_{\rm ped} \gg \chi_{\rm i,turb}, D_{\rm turb}$ in the H-mode pedestal and $\chi_{\rm i,neo}, D_{\rm ped} \ll \chi_{\rm i,turb}, D_{\rm turb}$ for the L-mode turbulence. $p_{\rm turb}$ is the pressure for L-mode, while $p_{\rm neo}$ is the pressure in the pedestal. Therefore, the hysteresis surely tracks Nu scaling, as shown in Fig. 6.

In the same manner, we estimate the strength of hysteresis in ion temperature and density, by using the ratios of the pedestal and L-mode gradient scale lengths, $P_{T_i} \equiv L_{T_i,\rm ped}^{-1}/L_{T_i,\rm turb}^{-1}$ and $P_n \equiv L_{n,\rm ped}^{-1}/L_{n,\rm turb}^{-1}$, yielding

$$P_{T_i} = P_p\left(\frac{1 - \varepsilon_{\rm ped}/{\rm Pr}_{\rm ped}}{1 - \varepsilon_{\rm turb}}\right) \sim {\rm Nu}, \tag{15}$$

$$P_n = P_p\left(\frac{1 + \varepsilon_{\rm ped}/{\rm Pr}_{\rm ped}}{1 + \varepsilon_{\rm turb}}\right) \sim {\rm Nu}, \tag{16}$$

where $\varepsilon_{\rm ped} = ST_{\rm i,ped}/Q$, and $\varepsilon_{\rm turb} = ST_{\rm i,turb}/Q$. The hystereses in temperature and density also scales with Nu, but the scalings are different for gradients and quantities.

VI. SUMMARY AND REMARKS

Since studies of transport and transition dynamics in vigorously heated plasma near the power threshold are both scientifically and pragmatically important, we have studied the spatio-temporal dynamics of the H → L back transition using a one-dimensional transport and turbulence model. After increasing the power above the threshold and then decreasing heat flux, we observed the L → H → L transition to occur via a limit-cycle oscillation phase, i.e., the I-phase. The duration of the I-phase is variable. The specific results of this study are

(i) The system will revisit I-phase for slow power ramp down. Thus, the observed back-transition D_α oscillations are not necessarily "ELMs," but rather oscillations which are part of the back-transition LCO dynamics.
(ii) In the model, I-phase nucleates at the pedestal shoulder in the back transition, as this is the site of the residual turbulence in H-mode.
(iii) Fast ramp-downs reveal a single burst of zonal flow activity. This is similar to results for fast ramp-ups in forward transitions. Thus, the "landing" is not always "soft."
(iv) The back-transition relaxation drives ∇p_i oscillations and thus triggers bursts of D_α. This physics is clearly different from that of ELMs, due to MHD instabilities.

Note that in the back-transition LCO observed in DIII-D (Fig. 1), the experimental signatures of MHD event preceding the back-transition LCO are identical to the Type-I ELMs. The ELM seems to flatten the upper pedestal and reduces the diamagnetic shear in the region of the residual turbulence. Then, turbulence is driven and drives zonal flow and LCO occurs.

Regarding feedback loop structure, the advance of the turbulence front is the key physical process. As illustrated in Fig. 4, a self-reinforcing feedback-loop mechanism is identified as

(i) a drop in heat flux Q, followed by
(ii) a decrease in ∇p and ∇n,
(iii) a decrease in $\langle v_E \rangle'^2$, followed by
(iv) the invasion of the quiescent zone by turbulence
(v) an increase in transport, followed by
(vi) a drop in ∇p and ∇n, which returns to (ii), above, and thus closes the loop.

Two open questions concerning phenomenology here are:

(i) how much invasion of turbulence by spreading processes actually occurs before complete collapse of the pedestal?,
(ii) does the observed threshold power for back transition P_{Th} correspond to that for which the spreading front penetrates all the way to the LCFS?

There questions will be addressed in a future paper.

We summarize the analyses of hysteresis and discuss their implications for experiment. Model studies indicate:

(i) hysteresis in length scale tracks Nu, as expected. Hysteresis in length scale or profile gradient is stronger than for profile quantity, (i.e., hysteresis in L_p^{-1} or ∇p stronger than for p). Further study of hysteresis near criticality is required.
(ii) relative hysteresis of ∇n and ∇T_i is observed, and is proportional to $\mathrm{Pr}_{\mathrm{ped}}^{-1} = \chi_{\mathrm{i,neo}}/D_{\mathrm{ped}}$. Thus, we expect the H-mode to be more resilient in L_n^{-1} than in $L_{T_i}^{-1}$.
(iii) different quantities $(T, L_T^{-1}, \cdots)$ exhibit different hysteresis behavior. Scale length hysteresis seems more fundamental than quantity hysteresis, as scale lengths are more directly linked to the driving flux.
(iv) hysteresis is linked to pedestal profile structure, since the back transition develops from the pedestal shoulder.

Some of the implications of our results for experiment are:

(i) studies of ELM-free back transitions would be illuminating, so as to isolate transport physics from MHD physics.
(ii) fluctuation studies during the back transition should track the turbulence invasion front, and attempt to determine the lag, if any, between changes in $E \times B$ shear and changes in intensity.
(iii) regarding the important subject of hysteresis
  - the measurement of hysteresis, as we defined in terms of profile gradients, would be beneficial to understanding of pedestal dynamics, since experimental measurement of Nu and $\mathrm{Pr}_{\mathrm{ped}}$ are not yet well organized.
  - hysteresis should be characterized in terms of *local* physical quantities. Studies of scale length hysteresis vs Nu would be especially illuminating.
  - relative hysteresis studies of $1/L_{T_i}$ vs $1/L_n$ and $1/L_{T_i}$ vs $1/L_{V_\phi}$ would be interesting, both on their own account and for their implications concerning, pedestal transport.
  - back-transition I-phase dynamics should be studied in connection with hysteresis.

We conclude this paper with the observation that *back* transition dynamics is an *ideal* testing ground for this or any other model. This is because the lack of data on, and experience with, back transitions necessarily forces the model to function in *predictive*, rather than *explanatory*, mode! Predictive tests of models against back transition phenomenology should be pursued.

ACKNOWLEDGMENTS

The authors acknowledge stimulating discussions with C. Hidalgo, S.-H. Hahn, A. Hubbard, H. Jhang, G. McKee, G.S. Xu, M. Xu, Z. Yan, and K.J. Zhao. This work was supported by the WCI Program of the National Research Foundation of Korea funded by the Ministry of Education, Science and Technology of Korea [WCI 2009-001] and the Department of Energy under Award Nos. DE-FG02-04ER54738, DE-DG02-08ER54984, and DE-FC02-04ER54698, General Atomics UCLA subcontract SC 45000041234 and CMTFO.

[1]C. Gormezano, A. C. C. Sips, T. C. Luce, S. Ide, A. Becoulet, X. Litaudon, A. Isayama, J. Hobirk, M. R. Wade, T. Oikawa *et al.*, Nucl. Fusion **47**, S285 (2007).
[2]K. Miki, P. H. Diamond, O. D. Gurcan, G. R. Tynan, T. Estrada, L. Schmitz, and G. S. Xu, Phys. Plasmas **19**, 092306 (2012).
[3]L. Schmitz, L. Zeng, T. L. Rhodes, J. C. Hillesheim, G. R. McKee, Z. Yan, W. A. Peebles, R. J. Groebner, K. H. Burrell, G. R. Tynan, E. J. Doyle, and G. Wang, in 39th EPS Conference and 16th International Congress on Plasma Physics, Stockholm, Sweden, 2012.
[4]D. M. Thomas, R. J. Groebner, K. H. Burrell, T. H. Osborne, and T. N. Carlstrom, Plasma Phys. Controlled Fusion **40**, 707 (1998).
[5]F. Ryter, M. Willensdorfer, P. Sauter, E. Viezzer, E. Wolfrum, R. Fischer, R. McDermott, T. Pütterich, and ASDEX Upgrade Team, in ITPA T&C Workshop, Hefei, China, 2012.
[6]F. L. Hinton, Phys. Fluids B: Plasma Physics **3**, 696 (1991).
[7]A. E. Hubbard, B. A. Carreras, R. L. Boivin, J. W. Hughes, E. S. Marmar, D. Mossessian, and S. J. Wukitch, Plasma Phys. Controlled Fusion **44**, A359 (2002).
[8]G. Bertotti, *Hysteresis in Magnetism: For Physicists, Materials Scientists, and Engineers*, Electromagnetism Series (Academic Press, Inc., 1998).
[9]K. Ida, M. Yoshinuma, K. Nagaoka, M. Osakabe, S. Morita, M. Goto, M. Yokoyama, H. Funaba, S. Murakami, K. Ikeda, H. Nakano, K. Tsumori, Y. Takeiri, O. Kaneko, and LHD Experiment Group, Nucl. Fusion **50**, 064007 (2010).
[10]S. Kim, H. Jhang, P. Diamond, L. Terzolo, S. Yi, and T. Hahm, Nucl. Fusion **51**, 073021 (2011).
[11]E.-J. Kim and P. H. Diamond, Phys. Rev. Lett. **90**, 185006 (2003).
[12]P. Manz, G. S. Xu, B. N. Wan, H. Q. Wang, H. Y. Guo, I. Cziegler, N. Fedorczak, C. Holland, S. H. Muller, S. C. Thakur, M. Xu, K. Miki, P. H. Diamond, and G. R. Tynan, Physi. Plasmas **19**, 072311 (2012).
[13]K. Zhao *et al.*, in *Proceedings of the 24th IAEA Fusion Energy Conference, San Diego, USA* (2012), pp. IAEA-CN-197/EX/7-2Ra.
[14]T. Estrada, C. Hidalgo, and T. Happel, Nucl. Fusion **51**, 032001 (2011).
[15]D. McDonald, private communication (2011).
[16]M. A. Malkov and P. H. Diamond, Phys. Plasmas **15**, 122301 (2008).
[17]The barrier width is mainly determined by the (fixed) boundary condition on p and n, heating and fueling parameters. With the parameters used in Ref. 2, typical barrier width is about $0.1(r/a)$.